ACS APPLIED MATERIALS & INTERFACES

www.acsami.org

Research Article

Adhesion Between MXenes and Other 2D Materials

Yanxiao Li, Shuohan Huang,[⊥] Congjie Wei,[⊥] Dong Zhou, Bo Li, Chenglin Wu,* and Vadym N. Mochalin*

Cite This: *ACS Appl. Mater. Interfaces* 2021, 13, 4682−4691

Read Online

ACCESS | Metrics & More | Article Recommendations | Supporting Information

ABSTRACT: MXenes, a large family of two-dimensional (2D) early transition metal carbides and nitrides, have excellent electrical and electrochemical properties, which can also be explored in assemblies with other 2D materials, like graphene and transition metal dichalcogenides (TMDs), creating heterostructures with unique properties. Understanding the interaction mechanism between 2D materials is critical for the design and manipulation of these 2D heterostructures. Our previous work investigated the interaction between SiO_2 and two MXenes ($Ti_3C_2T_x$ and Ti_2CT_x). However, no experimental research has been done on MXene interlayer interactions and interactions in MXene heterostructures. Here, we used atomic force microscopy (AFM) with SiO_2 tip and $Ti_3C_2T_x$ and Ti_2CT_x MXene-coated tips, respectively, to measure the adhesion energies of graphene, $MoSe_2$, $Ti_3C_2T_x$, and Ti_2CT_x MXene with other 2D materials. The measured adhesion energies show that only the interfaces involving graphene demonstrate dependence on the number of material monolayers in a stack. Comparing 40 interacting pairs of 2D materials, the lowest adhesion energy (~0.27 J/m^2) was found for the interfaces involving $MoSe_2$ and the highest adhesion energy was observed for the interfaces involving $Ti_3C_2T_x$ (~1.23 J/m^2). The obtained set of experimental data for 2D interfaces involving MXenes provides a basis for a future in-depth understanding of adhesive mechanisms at interfaces between 2D materials, which is an important topic for the design of 2D heterostructures with controlled interfacial strength and properties.

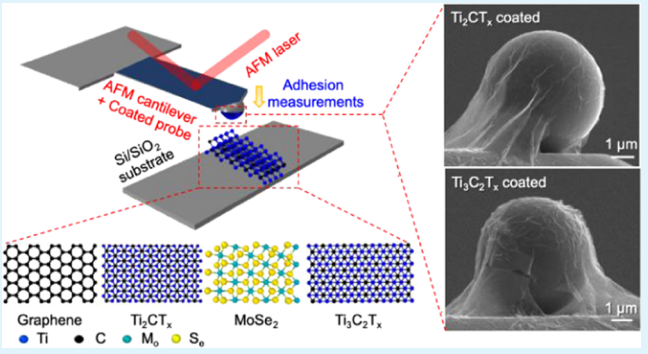

KEYWORDS: *transition metal dichalcogenides, $Ti_3C_2T_x$, Ti_2CT_x, MXenes, atomic force microscopy*

1. INTRODUCTION

The MXenes is a recently discovered and one of the largest families of two-dimensional (2D) materials.[1,2] MXenes have the chemical formula $M_{n+1}X_nT_x$ and consist of an early transitional metal (M), carbon or nitrogen (X), and surface-terminating groups (T), such as −F, −OH, −O, etc., where the unknown x denotes the fraction of the terminal groups in formulae.[3−5] MXenes can be delaminated using different intercalants like dimethyl sulfoxide (DMSO), tetraalkylammonium hydroxides (TBAOH), and lithium ions.[6−8] Due to their tailorable structures and properties, MXenes have shown great potential in optoelectronic devices,[9−17] supercapacitors,[18−25] and other energy conversion[26−29] and storage devices[8,30−37] made of van der Waals heterostructures of MXenes with other 2D materials, where interfacial adhesion is critical to the performance and reliability. However, most of the related research on MXene adhesion and interfacial properties is computational[38,39] with only a handful of experimental results that have become available over the past few years.[40]

Two-dimensional material nanobubbles[41] and atomic force microscopy (AFM) with a coated probe have been mostly used to measure adhesion energy at 2D material heterointerfaces.[42,43] Li et al. coated graphite onto the AFM probe through a dry transfer method to measure the adhesion between graphite and graphite, BN or MoS_2, respectively.[42] However, owing to a large thickness and high in-plane stiffness, the coated graphite film did not conform well to the spherical AFM tip, resulting in a corrugated surface. High irregularity in terms of surface profile led to inaccuracy in the estimated adhesion energy at the interface. Therefore, a direct coating of an AFM tip with more flexible 2D materials has been explored to avoid the surface profile irregularity induced by a thick layer.[43] So far, several approaches have been reported to coat graphene onto AFM tip[44−48] including: direct growth,[44,47] dry transfer approach[43,45,46] with polymers, and liquid phase exfoliation approach.[48] Each of these methods has its own advantages and disadvantages. Since MXenes are synthesized by selective etching from the MAX phase, the direct growth of

Received: October 19, 2020
Accepted: December 31, 2020
Published: January 12, 2021

https://dx.doi.org/10.1021/acsami.0c18624
ACS Appl. Mater. Interfaces 2021, 13, 4682−4691

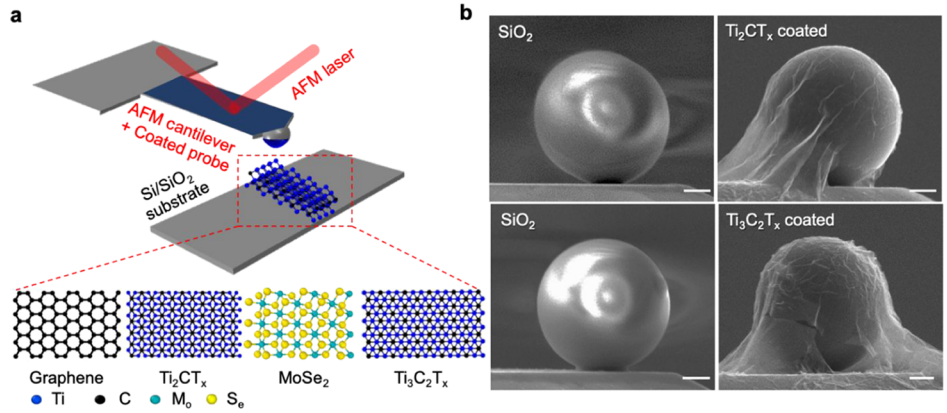

Figure 1. (a) AFM measurement schematic and (b) SEM images of AFM spherical probes before (left) and after (right) coating with Ti_2CT_x or $Ti_3C_2T_x$ MXenes, respectively (Scale bar: 1 μm).

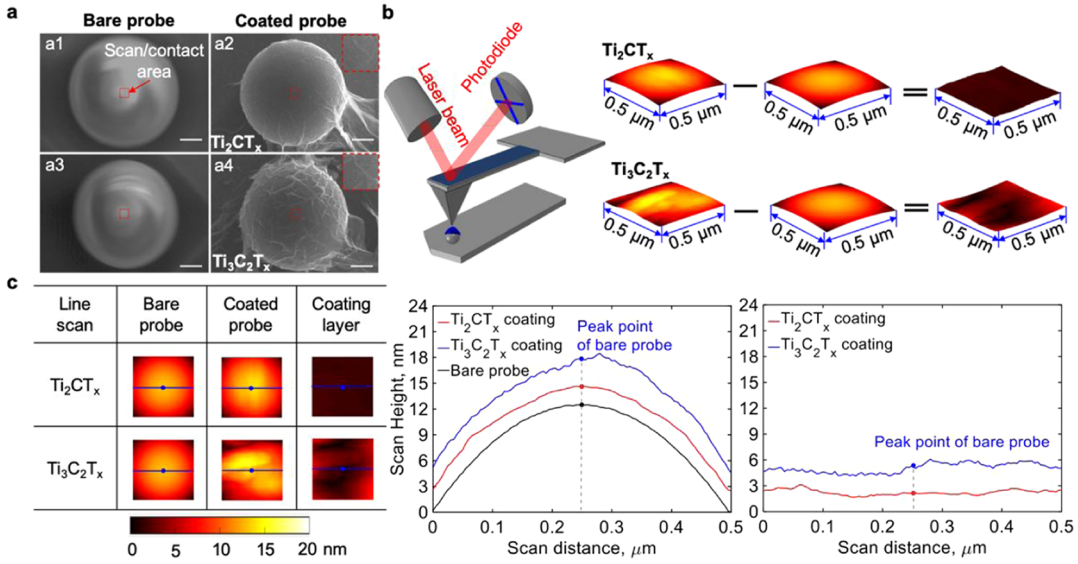

Figure 2. (a) SEM images of AFM spherical probes before and after coating with Ti_2CT_x or $Ti_3C_2T_x$ MXene (top view); insets are the zoomed-in images of the AFM scanning areas in tapping mode, scale bar: 1 μm. (b) AFM scanning setup in tapping mode and 3D profiles for bare probe, coated probe, and a coating layer. (c) Typical line scan profiles.

MXene on the AFM probe is not possible. In addition, the relatively large in-plane stiffness of MXene on polymers could lead to film delamination or fracture if a dry transfer method were used. In the interfacial film self-assembly method that we used, MXene will lay horizontally at the interface between water and toluene, which leads to conformal coating. This technique has been reported before[49] and was also adopted in our prior study,[50] where it yielded films with well-controlled thickness and surface roughness. Hence, we used an interfacial film self-assembly method to coat MXene on the spherical AFM probe in this work.

In this method, a spherical AFM probe is lifted through the self-assembled film of MXene flakes floating at the interface between water and toluene. The thickness of the coating can be controlled by adjusting the concentration of MXene colloidal solution. Due to the similarity between the AFM probe diameter (5 μm) and the size of MXene flakes (5−10 μm), wrinkling of the coating was effectively suppressed. Using the interfacial self-assembly, Ti_2CT_x or $Ti_3C_2T_x$ MXene was coated on the spherical AFM probes. The surface profile of the coated probe was mapped using another sharp AFM tip in the tapping mode Figure S1 to validate the conformality of the coating. Using both bare and MXene-coated probes in the contact mode of AFM (details discussed in Section 2.2), we were able to directly measure adhesion forces between the materials on the AFM probe (SiO_2 or a MXene) and substrate materials (graphene, $MoSe_2$, Ti_2CT_x, or $Ti_3C_2T_x$). The adhesion energy was evaluated from the adhesion force with the Rumpf model.[51,52] In this way, the adhesion energy values were obtained for a total of 60 interacting pairs, where 20 interacting pairs involving SiO_2/graphene, SiO_2/$MoSe_2$, and SiO_2/MXene interfaces were measured with a bare probe and 40 interacting pairs involving MXene/graphene, MXene/$MoSe_2$, and MXene/MXene interfaces were measured using a MXene-coated probe. Only the adhesion energy of interfaces involving graphene has shown a dependence on the number of material monolayers in a stack. Among the 40 interacting pairs of 2D materials, the lowest adhesion energy (~0.27 J/m^2) was found for interfaces with $MoSe_2$ and the highest adhesion energy was observed for interfaces involving $Ti_3C_2T_x$ (~1.23 J/m^2). Our large set of obtained experimental data for 2D interfaces involving MXenes provides a basis for an in-depth understanding of adhesive mechanisms at the interfaces in 2D heterojunctions. In addition, these results provide an important

https://dx.doi.org/10.1021/acsami.0c18624
ACS Appl. Mater. Interfaces 2021, 13, 4682−4691

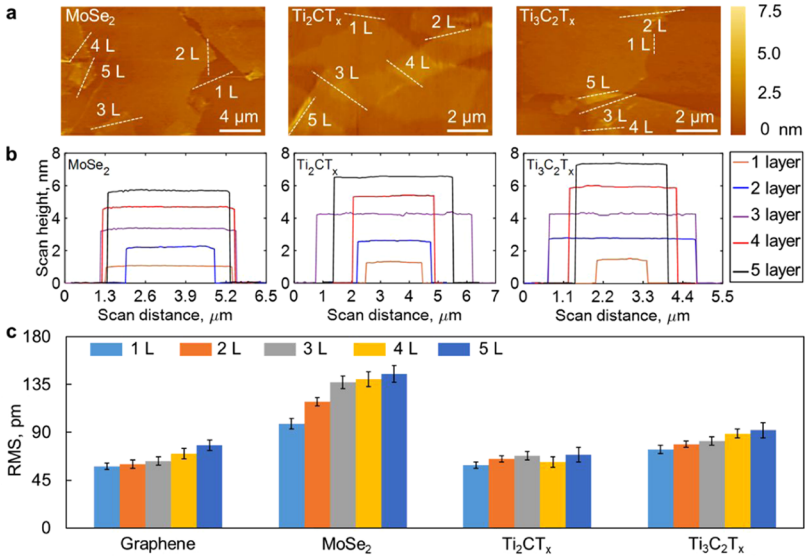

Figure 3. (a) AFM images of $MoSe_2$, Ti_2CT_x, and $Ti_3C_2T_x$ MXene films on the Si/SiO_2 substrate, (b) line scans for one- to five-layer $MoSe_2$, Ti_2CT_x, and $Ti_3C_2T_x$ MXene, correspondingly, and (c) RMS values with standard deviations for one- to five-layer graphene, $MoSe_2$, Ti_2CT_x, and $Ti_3C_2T_x$ MXene, correspondingly.

input for the design of 2D heterostructures with controlled interfacial strength.

2. RESULTS AND DISCUSSION

2.1. Tip and Substrate Surface Profiles. The adhesion measurements were performed using MXene (Ti_2CT_x or $Ti_3C_2T_x$)-coated spherical SiO_2 probes (5 μm diameter) and the corresponding planar substrates to form MXene/graphene, MXene/$MoSe_2$, and MXene/MXene interfaces as shown in Figure 1a. The scanning electron microscopy (SEM) images of AFM probes before and after coating are shown in Figure 1b.

To measure the thickness and surface roughness of the coating, a sharp Si/SiO_2 tip with 3 nm radius was used to scan the surfaces of the larger probes in tapping mode before and after coating (Figure 2a). The scanned area in the center of the tip was 0.5 μm × 0.5 μm (red dash frame) as determined by the projected contact area based on the interaction range between tip material and samples on the substrate (Figure S2). The coating layer profile was obtained by subtracting the scanning profile of the bare probe from that of the coated probe (Figure 2b). Average thickness values of 2.74 nm (root-mean-square (RMS) = 606 pm) and 5.90 nm (RMS = 610 pm) for Ti_2CT_x and $Ti_3C_2T_x$ coatings, respectively, were calculated from the extracted profiles (Figure 2c). The peak point position of the bare probe is labeled with a dot. These thickness values correspond to two monolayers in the Ti_2CT_x coating and three monolayers in the $Ti_3C_2T_x$ coating and were calculated using the corresponding d-spacing values (1.36 nm for Ti_2CT_x and 1.48 nm for $Ti_3C_2T_x$), as described before.[50] The d-spacing value for $MoSe_2$ is 1.17 nm, which is calculated from XRD results in ref 53, in which $MoSe_2$ was synthesized using the same method.

Surface profiles and roughness of one- to five-layer graphene, $MoSe_2$ flakes, Ti_2CT_x, and $Ti_3C_2T_x$ MXene flakes were also characterized using AFM in tapping mode. The number of stacked monolayers of graphene was obtained from Raman spectra. AFM images of the samples illustrating areas with a different number of monolayers of $MoSe_2$, Ti_2CT_x, and $Ti_3C_2T_x$ MXene are shown in Figure 3a. The line scans in Figure 3b show the relative height between the sample flake and the substrate. The number of monolayers was calculated by dividing the relative height with d-spacing of the material. The average RMS values shown in Figure 3c were obtained from the relative height curves in Figure 3b. Very low RMS values are indicative of smooth sample surfaces, which become slightly rougher with more flakes in a stack. RMS values for graphene and MXene are smaller than for $MoSe_2$.

2.2. Force−Displacement Response. A typical adhesion force versus displacement response measured with a one-layer graphene sample using a Ti_2CT_x-coated probe is shown in Figure 4a. During the approach stage, the cantilever beam experiences a negative bending followed by positive bending as the probe jumps in contact with the sample surface and is further pushed against the surface. During the subsequent withdrawal stage, the cantilever beam experiences a reverse bending history (I−IIIA or IIIB) until the probe jumps off (III)A or IIIB losing contact with the sample surface (IV). The

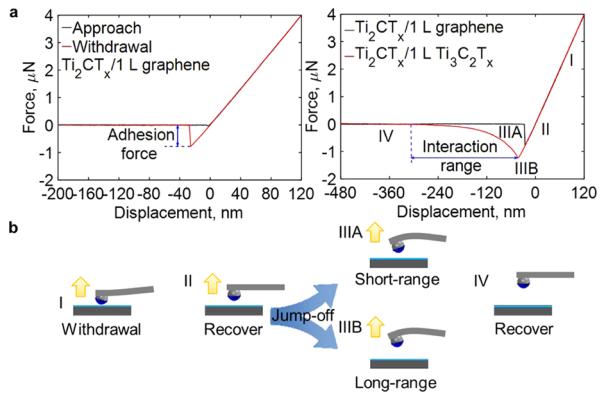

Figure 4. (a) Force versus displacement curves measured during probe approach and withdrawal for Ti_2CT_x/one-layer (1 L) graphene (left) and force versus displacement curves of probe withdrawal for Ti_2CT_x/1 L graphene and Ti_2CT_x/1 L $Ti_3C_2T_x$ (right). (b) Cartoons demonstrating the stages of bending of the AFM tip during the probe withdrawal.

https://dx.doi.org/10.1021/acsami.0c18624
ACS Appl. Mater. Interfaces 2021, 13, 4682−4691

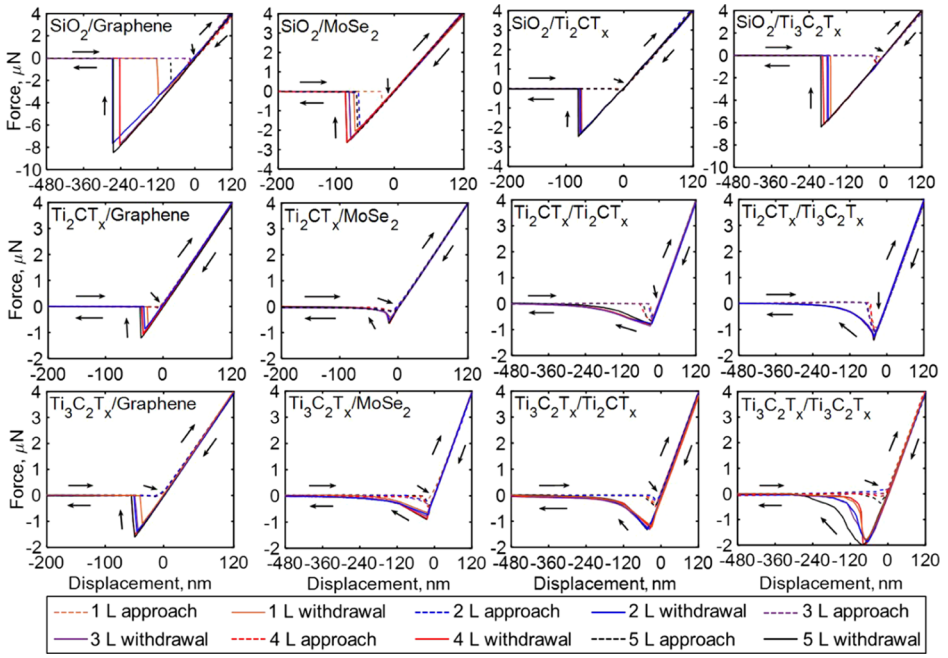

Figure 5. Approach and withdrawal curves for the probes coated with different materials (in front of the slash in sample names) and one to five layers of materials on the substrate (following the slash in sample names).

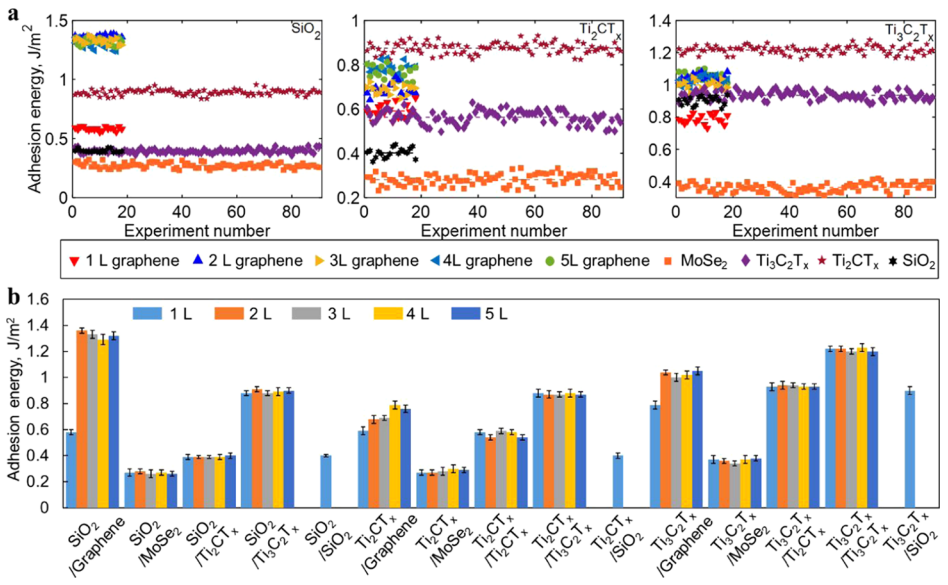

Figure 6. (a) Adhesion energies measured on one to five layers of a 2D material deposited on the SiO_2 substrate (symbols) and the material coated on the tip (indicated in each chart title) with average values shown by horizontal lines, and (b) bar chart of average adhesion energies with standard deviations (X-axis labels: material coated on the tip/material deposited on the SiO_2 substrate).

maximum interaction force during the probe withdrawal was assigned as the adhesion force between the probe and the sample surface. The interaction range was defined as the difference between the displacement corresponding to jump-off (point IIIA or IIIB in Figure 4a) and the displacement at full recovery corresponding to zero force (point IV in Figure 4a). It is interesting to point out that significant differences were observed in both adhesion forces and, especially, the interaction ranges among different material pairs. For instance, Ti_2CT_x (probe)/one-layer $Ti_3C_2T_x$ (substrate) has shown 1.60 times adhesion force and 162.62 times the interaction range of Ti_2CT_x (probe)/one-layer graphene (substrate) (Figure 4b).

All force versus displacement curves for different material interaction pairs are shown in Figure 5. For each interaction pair, responses registered with monolayers, as well as stacks of monolayers are shown together. The adhesion force measured between the tip and one-layer graphene is much lower than for two- to five-layer graphene. However, in contrast to graphene, no number-of-monolayer dependence was found for the maximum adhesion force measured with $MoSe_2$ or MXene samples. Average adhesion forces with the corresponding standard deviations are shown in Table S1. It was found that the average adhesion forces of $Ti_3C_2T_x$ in contact with other 2D materials studied here are higher than with Ti_2CT_x or $MoSe_2$. Long-range interactions during jump-off were observed

https://dx.doi.org/10.1021/acsami.0c18624
ACS Appl. Mater. Interfaces 2021, 13, 4682−4691

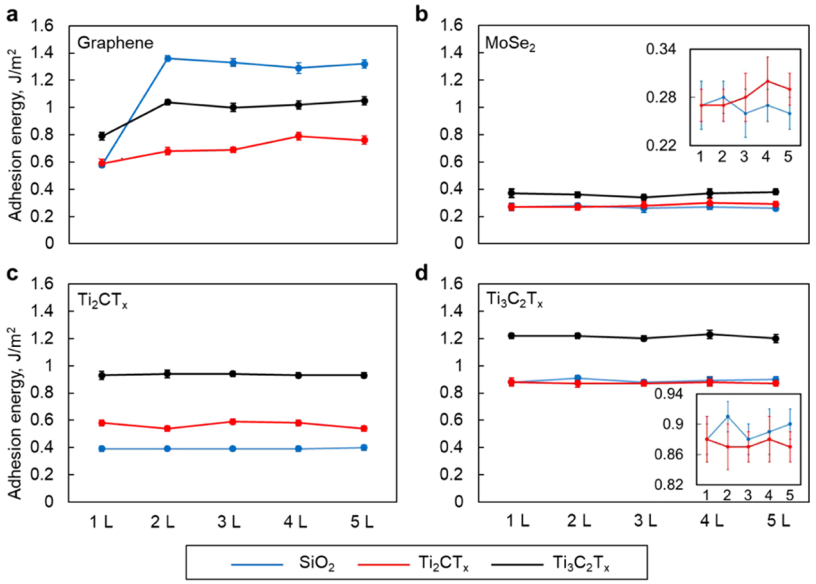

Figure 7. Average adhesion energies and their standard deviations measured with SiO_2-, Ti_2CT_x-, and $Ti_3C_2T_x$-coated probes (legend) on one- to five-layer (a) graphene, (b) $MoSe_2$-, (c) Ti_2CT_x-, and (d) $Ti_3C_2T_x$-coated substrates. The insets are the results measured with the SiO_2 probe or the Ti_2CT_x-coated probe.

between a MXene-coated probe and MXene or $MoSe_2$ substrates.

2.3. Adhesion Energy and Interaction Range. The adhesion energy was calculated from the measured adhesion force using the modified Rumpf model, which is valid when RMS is less than 20 nm[54]

$$W_{adh} = \left(\frac{F_{adh}}{\lambda\pi R_{tip}}\right) \frac{\left(1 + \frac{R_{tip}}{1.48RMS_{sub}}\right)^{-1} + \left(1 + \frac{1.48RMS_{sub}}{Z_0}\right)^{-2}}{\left(1 + \frac{R_{tip}}{1.48RMS_{tip}}\right)^{-1} + \left(1 + \frac{1.48RMS_{tip}}{Z_0}\right)^{-2}} \quad (1)$$

where W_{adh} is the adhesion energy per unit area, F_{adh} is the maximum adhesion force measured during the withdrawal stage, R_{tip} is the tip radius, RMS_{sub} is the RMS value for the surface of the sample deposited on substrate, RMS_{tip} is the RMS value for the sample surface deposited on the tip, and Z_0 is the equilibrium separation of the two surfaces. The equilibrium separation Z_0 is defined as zero-force distance between the surface of the Si/SiO_2 tip or MXene-coated tip and the sample surface, which for our experiments was estimated to be 0.3 nm. λ is an effective coefficient that depends on the model and data used (Table S2, see ref 50 for further details). In our experiments, RMS values for the coated probe are 607 pm (Ti_2CT_x coating) and 610 pm ($Ti_3C_2T_x$ coating), for uncoated probe the RMS value is 180 pm, and for one- to five-layer stacks of different materials on the substrate the values are shown in Figure 3c. All adhesion energies in this work were calculated according to eq (1). Gaussian fitting was applied to obtain the average adhesion energy and standard deviations for each specimen (Figure S3). Adhesion energies between all studied surfaces are presented in Table S3. All calculated adhesion energies with the average adhesion energies measured using SiO_2-, Ti_2CT_x - or $Ti_3C_2T_x$-coated probes are shown in Figure 6a. Eighteen measurements were conducted for each interaction pair. Most of the adhesion energy values produced in these measurements fluctuate within less than 5% of the average value, indicating a good consistency of the measurements. The average adhesion energies with standard deviations are shown in Figure 6b and are plotted against the number of monolayers for all interaction pairs in Figure 7. When the material deposited on the substrate is graphene, the adhesion energy increases as the number of stacked graphene monolayers increases from 1 to 2 (0.58 ± 0.02 to 1.36 ± 0.02 J/m^2 for SiO_2 probe, 0.59 ± 0.03 to 0.68 ± 0.03 J/m^2 for Ti_2CT_x-coated probe, and 0.79 ± 0.03 to 1.04 ± 0.02 J/m^2 for $Ti_3C_2T_x$-coated probe). However, this trend ceases for three or more stacked graphene monolayers. Interestingly, no number-of-monolayer effect was observed when the material on the substrate is $MoSe_2$, Ti_2CT_x, or $Ti_3C_2T_x$. The thickness dependence of adhesion for the graphene interface has been explained in our previous paper.[50] Briefly, graphene monolayer is thinner than MXene and $MoSe_2$, and thus, in the case of graphene stacks, the van der Waals interaction range is not limited by the topmost layer but also propagates down to the second topmost layer. In addition, the increased adhesion energy for graphene with an increasing number of layers was also reported by others.[55]

In addition, when the substrate material is $MoSe_2$, Ti_2CT_x or $Ti_3C_2T_x$, the adhesion energies measured with $Ti_3C_2T_x$-coated probe (black lines in Figure 7a–d) are higher than those measured with the Ti_2CT_x-coated probe (red lines in Figure 7a–d), which are in turn close to the values measured with the bare SiO_2 probe (blue lines in Figure 7a–d). The fact that the adhesion of $Ti_3C_2T_x$ is generally higher than that of Ti_2CT_x could be due to the differences in the atomic structure. The additional layers of Ti and C atoms in a thicker MXene monolayer can change the surface polarization and in turn the adhesion energy. In addition, atomic vacancies for these two MXenes could be different, which cannot be quantified easily especially for Ti_2CT_x due to its high chemical reactivity.

The interaction ranges (defined in force–displacement response section) for different contact pairs are shown in

https://dx.doi.org/10.1021/acsami.0c18624
ACS Appl. Mater. Interfaces 2021, 13, 4682–4691

Table 1. Interaction Range (nm)

substrate tip	number of monolayer	graphene	$MoSe_2$	Ti_2CT_x	$Ti_3C_2T_x$
SiO_2	1 layer	1.75 ± 0.11	2.41 ± 0.14	1.38 ± 0.13	1.52 ± 0.14
	2 layers	1.72 ± 0.13	2.46 ± 0.16	1.39 ± 0.12	1.49 ± 0.12
	3 layers	1.76 ± 0.09	2.51 ± 0.11	1.35 ± 0.15	1.43 ± 0.13
	4 layers	1.74 ± 0.12	2.45 ± 0.13	1.33 ± 0.14	1.48 ± 0.15
	5 layers	1.70 ± 0.10	2.56 ± 0.15	1.44 ± 0.14	1.57 ± 0.14
Ti_2CT_x	1 layer	1.71 ± 0.13	60.95 ± 2.15	335.26 ± 16.52	278.08 ± 10.03
	2 layers	1.75 ± 0.17	57.88 ± 2.82	336.03 ± 17.82	275.23 ± 16.24
	3 layers	1.77 ± 0.12	57.26 ± 2.63	318.45 ± 18.71	278.22 ± 13.02
	4 layers	1.76 ± 0.14	58.30 ± 2.54	329.03 ± 17.64	277.10 ± 14.03
	5 layers	1.73 ± 0.13	58.29 ± 2.92	331.38 ± 16.52	277.73 ± 15.02
$Ti_3C_2T_x$	1 layer	1.79 ± 0.29	258.63 ± 13.03	273.12 ± 13.13	208.42 ± 10.82
	2 layers	1.81 ± 0.22	256.60 ± 12.84	288.20 ± 12.56	215.48 ± 11.20
	3 layers	1.79 ± 0.25	257.21 ± 13.29	279.00 ± 14.22	228.55 ± 11.34
	4 layers	1.76 ± 0.27	264.59 ± 11.23	274.20 ± 15.68	223.50 ± 12.72
	5 layers	1.74 ± 0.23	268.11 ± 14.22	291.00 ± 14.83	215.62 ± 10.67

Table 1. Short-range interactions (<10 nm) were observed for SiO_2/(graphene, $MoSe_2$, Ti_2CT_x, $Ti_3C_2T_x$), Ti_2CT_x/graphene, and $Ti_3C_2T_x$/graphene. Long-range interactions (>30 nm) were observed for other pairs, which do not involve SiO_2 or graphene. It is worth noting here that the interaction range becomes significantly longer (208.42−336.03 nm) when both the probe and substrate coating materials are MXenes.

Combining the adhesion energy and interaction range data, we see that the interaction pairs involving SiO_2 and graphene have a relatively short interaction range (<3 nm), indicating that in these cases the adhesion force is dominated by the van der Waals interactions.

However, when the probe and substrate materials are MXenes, the long interaction ranges are more typical, which indicates possible water bridging. Although all MXenes were dried in ambient air at 6% RH prior to measurements, it is possible that a small amount of water still remains and even more was adsorbed during the measurements due to a strong hydrophilicity of MXenes also discovered by other researchers.[56,57] In particular, Persson et al. have recently reported that water chemisorbed on the MXene surface cannot be removed even after preheating the sample under vacuum at 700 °C.[57] Our experimental data and literature reports, therefore, point to the presence of a notable amount of strongly bonded water on MXene surfaces. Since it is difficult or nearly impossible to completely remove this water, it should be accounted as an intrinsic part of the material for most of its practical applications and, therefore, its role in adhesion, friction, etc., should be considered as an intrinsic property of MXenes. In particular, when two MXene surfaces are brought in contact, the formation of water bridges between them seems to be unavoidable in ambient conditions, which in this study manifested itself through an extremely long interaction range between the MXene surfaces. However, this water-bridging effect does not occur with SiO_2/MXene, and MXene/graphene interfaces, possibly due to the more hydrophobic nature of SiO_2 and graphene and much higher hydrophilicity of the MXenes.

3. EXPERIMENTAL SECTION

3.1. Atomic Force Microscopy (AFM). AFM (Innova, Bruker) was conducted at room temperature and 6% relative humidity (RH). Thin films of graphene, $MoSe_2$ or MXene were deposited on a silicon substrate covered with a thin (~300 nm) layer of spontaneously formed silicon oxide. The static eliminator (Static Sensing Ionizer, Keyence) was used to neutralize any interfering electrostatic charges on the sample and/or AFM tip. Typically, 2.5 μm radius spherical silicon probes coated with films of two different MXenes were used to measure adhesive behavior between the tip and substrate materials. In the films of each material formed on the substrate by random stacking of 2D material flakes, we have identified small areas corresponding to stacks of a given number of monolayers (1 to 5) and have performed 18 measurements in each of these areas. The cantilever stiffness provided by the supplier (Appnano, Inc.) is ~33 N/m. The force−displacement responses for the approach and withdrawal stages were recorded and analyzed. To avoid oxidation of MXenes,[50] all MXene samples were measured within no more than 12 h from the time of their preparation and drying (as described below).

3.2. Synthesis of Graphene and the Preparation of Graphene Samples on Si Wafers. Large-area monolayer graphene was grown by chemical vapor deposition (CVD) on 2 cm × 10 cm copper foils (Alfa Aesar, CAS: 7440−50−8, LOT No. P17D009). During this process, gas species were fed into the reactor flow over the 25 μm thick piece of copper foil, where hydrocarbon precursors decomposed to carbon radicals at the copper surface and then formed monolayer graphene. To prepare the multilayer graphene, a copper foil with graphene on top was spin-coated with a layer of poly(methyl methacrylate) (PMMA) (4000 rpm for 30 s). The foil was then etched away in 0.2 mol L^{-1} $FeCl_3$ and 0.2 mol L^{-1} $(NH4)_2S_2O_8$ for 2 h. The remaining graphene/PMMA was cleaned with deionized water, transferred onto freshly synthesized graphene on copper foil and heated at 50 °C in dry air to remove water. After another copper foil etching process, the graphene/graphene/PMMA sample was obtained. The three- to five-layer graphene stacks were prepared by repeating this procedure. The PMMA with attached graphene stacks were then transferred onto target Si(111)/SiO_2 substrates and baked at 120 °C for 15 min to reduce a possible strain mismatch caused by the transfer. Prior to transfer, Si substrates were cleaned by 30 min bath sonication in acetone and hydrophilized in piranha solution (3 mL 30% H_2O_2 slowly added to 9 mL 98% H_2SO_4) for 12 h, followed by thorough rinsing with deionized water. Finally, PMMA was dissolved in acetone, yielding a sample of graphene on the Si/SiO_2 substrate. The residue of the polymer was etched away at 400 °C in hydrogen.

3.3. Synthesis of MAX Phases. Ti_3AlC_2 was prepared by the pressureless synthesis method. The as-received powders of titanium (−325 mesh, 99%, Alfa Aesar), aluminum (−325 mesh, 99.5%, Alfa Aesar), and graphite (−325 mesh, 99%, Alfa Aesar) were ball-milled in 3:1.1:1.88 molar ratio in a polyethylene jar for 12 h at 100 rpm. Afterwards, the mixture was sintered at 1550 °C for 2 h in Ar flow in an alumina boat using a tube furnace (GSL-1800X -KS60-UL, MTI

https://dx.doi.org/10.1021/acsami.0c18624
ACS Appl. Mater. Interfaces 2021, 13, 4682−4691

Corporation). For Ti_2AlC synthesis, the as-received powders of titanium carbide (typically 2 μ size, 99.5%, Alfa Aesar), titanium (−325 mesh, 99%, Alfa Aesar), and aluminum (−325 mesh, 99.5%, Alfa Aesar) were ball-milled in a molar ratio of 0.85:1.15:1.05. The mixture was then heated at 1400 °C for 4 h under Ar flow in an alumina boat. The resulting ceramics were manually crushed into powders using mortar and pestle.

3.4. Preparation of MXene Thin Films on Si Wafers. $Ti_3C_2T_x$ MXene was synthesized by selective etching of Al from Ti_3AlC_2. The etching was done by slowly mixing 0.3 g of Ti_3AlC_2 (−325 mesh, particle size ≤ 45 μm) to the etchant, prepared by dissolving 0.3 g LiF in 6 mL of 6 M HCl in a 50 mL plastic centrifuge tube.[58] The mix was stirred for 24 h at room temperature, followed by repeated washing with deionized water and centrifugation until the pH of supernatant reached 5.5−6.0. $Ti_3C_2T_x$ aqueous colloidal solution was obtained via 5 min hand-shaking followed by 1 h centrifugation at 3500 rpm. $Ti_3C_2T_x$ thin films on Si were prepared from the concentrated $Ti_3C_2T_x$ colloidal solutions via the interfacial film deposition method.[49,50] To prepare MXene thin films, 50−300 μL of $Ti_3C_2T_x$ colloidal solution was mixed in 50 mL of deionized water (DI) water together with 3−6 mL toluene added during 15 min of vigorous stirring. The dispersion was then poured directly into a beaker filled with 400 mL of DI water and with a few pieces of precleaned Si wafers placed at the bottom. After ∼20 min standing still, the $Ti_3C_2T_x$ film was self-assembled at the interface between water and toluene, and then the pieces of Si wafers were slowly lifted up from the solution through the interface, catching the interfacial MXene film. Finally, the MXene-coated Si wafers were dried for 12 h in Ar flow at room temperature to avoid oxidation. Ti_2CT_x colloidal solutions, as well as thin films, were obtained using the same methods, except the MAX phase in this case was Ti_2AlC (−325 mesh, particle size ≤ 45 μm) and the MXene (Ti_2CT_x) film drying time was 4 h in Ar flow at room temperature. The adhesion measurements were carried out immediately after the films were dried.

3.5. Synthesis of $MoSe_2$. $MoSe_2$ was synthesized using chemical vapor deposition.[59] Briefly, 700 mg of selenium (Se) (Sigma-Aldrich) and 15 mg of molybdenum oxide (MoO_3) powder (Sigma-Aldrich) were used as the Se and Mo precursors. The MoO_3 crucible was put at the center of a 2 inch fused quartz tube, and Se was located in the upstream region, which was 7.5 inches away from the MoO_3 crucible. A single side polished Si/SiO_2 was used as the growth substrate placed upon the MoO_3 crucible with the polished side facing the crucible's bottom. The heating rate and the growth temperature were 50 °C/min and 760 °C, respectively. Ar/H_2 (15% H_2) was used as the carrier gas at a flow rate of 35 SCCM. After 10 min growth, the furnace was cooled down to room temperature naturally, and the flow of Ar/H_2 was maintained during the cooling.

3.6. Raman Spectroscopy. Raman spectroscopy was performed to analyze one- to five-layer graphene and $MoSe_2$. Renishaw InVia confocal Raman microspectrometer with 532 nm laser, 20× objective, and a 1200 l mm^{-1} grating was used for the measurements. The spectra were acquired with 10 s exposure time, 10% of laser power, and three accumulations.

Graphene is characterized by G band at ∼1580 cm^{-1} and 2D band at ∼2700 cm^{-1}.[60] Raman spectra (Figure S4) of our graphene samples exhibited typical characteristics of high-quality graphene with the I_G/I_{2D} ratio 0.3−3. Raman spectroscopy and calculation of the number of MXene monolayers were reported before.[50]

The Raman spectrum of $MoSe_2$ is shown in Figure 8. The as-grown $MoSe_2$ exhibits several typical signatures in the range of Raman shifts from 200 to 360 cm^{-1}. These results agree well with former reports.[61−63]

4. CONCLUSIONS

We report experimental measurements of adhesion force and interaction range for contacts involving one of two different MXenes and other 2D materials, using MXene-coated spherical AFM probes in contact mode. The highest adhesion energy was found for the $Ti_3C_2T_x/Ti_3C_2T_x$ interface (1.23 J/m^2). The lowest (0.27 J/m^2) for the $Ti_3C_2T_x/MoSe_2$ interface. The longest interaction range was found for the Ti_2CT_x/Ti_2CT_x interface (336.03 nm); the shortest was found for the Ti_2CT_x/graphene interface (1.71 nm), as shown in Figure 9. The water-bridging adhesion mechanism is suspected for MXene/$MoSe_2$ and MXene/MXene interfaces even at a low RH level, indicating the unique adhesive behavior of MXenes among other 2D materials.

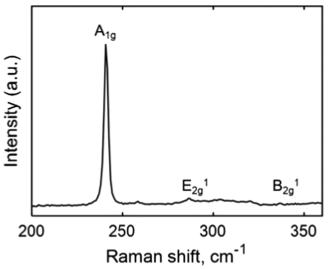

Figure 8. Raman spectrum of $MoSe_2$ on the SiO_2 substrate.

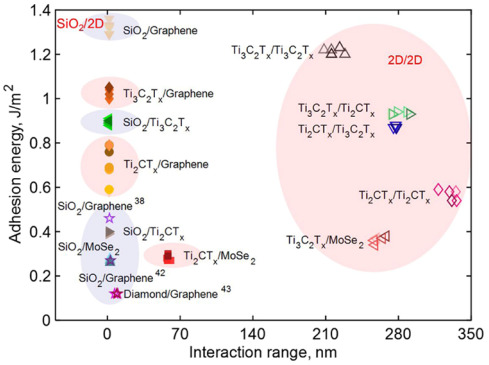

Figure 9. Adhesion energy-versus interaction range (red background: 2D material interfaces, blue background: 2D material and SiO_2 or diamond interfaces). Numerical values from refs 52, 64 and 65 are incorporated for comparison.

The number-of-monolayer effect was only observed for interactions involving graphene, while MXenes showed no signs of such dependence, similar to our prior observations of adhesion between MXenes and SiO_2.[50] The reported data show the possibility of designing 2D heterostructures with MXene layers acting as a "glue" that combines high interfacial adhesion with long interaction ranges with respect to other MXenes and 2D materials. These findings will lead to a better design of 2D homo- and heterostructures for optoelectronic, MEMS, and other applications. Moreover, this work further demonstrates AFM as a viable technique for studying adhesion between 2D materials experimentally at the nanoscale.

■ ASSOCIATED CONTENT

Supporting Information

The Supporting Information is available free of charge at https://pubs.acs.org/doi/10.1021/acsami.0c18624.

Adhesion forces between all studied surfaces; λ values between all studied surfaces; adhesion energy values between all studied surfaces; illustration of the tapping mode of AFM imaging; illustration of the AFM probe scan area in tapping mode; adhesion energy histograms with Gaussian fits for all adhesion energy results; and Raman spectra (PDF)

https://dx.doi.org/10.1021/acsami.0c18624
ACS Appl. Mater. Interfaces 2021, 13, 4682−4691

AUTHOR INFORMATION

Corresponding Authors

Chenglin Wu − *Department of Civil, Architectural, and Environmental Engineering, Missouri University of Science and Technology, Rolla, Missouri 65401, United States;* orcid.org/0000-0001-7733-1084; Email: wuch@mst.edu

Vadym N. Mochalin − *Department of Chemistry and Department of Materials Science and Engineering, Missouri University of Science and Technology, Rolla, Missouri 65401, United States;* orcid.org/0000-0001-7403-1043; Email: mochalinv@mst.edu

Authors

Yanxiao Li − *Department of Civil, Architectural, and Environmental Engineering, Missouri University of Science and Technology, Rolla, Missouri 65401, United States*

Shuohan Huang − *Department of Chemistry, Missouri University of Science and Technology, Rolla, Missouri 65401, United States*

Congjie Wei − *Department of Civil, Architectural, and Environmental Engineering, Missouri University of Science and Technology, Rolla, Missouri 65401, United States*

Dong Zhou − *Department of Mechanical Engineering, Villanova University, Villanova, Pennsylvania 19085, United States*

Bo Li − *Department of Mechanical Engineering, Villanova University, Villanova, Pennsylvania 19085, United States;* orcid.org/0000-0001-9766-7925

Complete contact information is available at: https://pubs.acs.org/10.1021/acsami.0c18624

Author Contributions

⊥S.H. and C.W. contributed equally to the first author.

Author Contributions

Y.L., S.H.H., and C.J.W. contributed equally to this work. C.L.W., V.N.M., and B.L. conceived and supervised the project, designed the experiments, and guided the team; Y.X.L. synthesized graphene, performed characterization, as well as adhesion measurements and data analysis; S.H.H. sythethesized $Ti_3T_2T_x$ and Ti_2CT_x MXenes and performed sample characterization; C.J.W. carried out an analysis of adhesion measurements. D.Z. sythethesized $MoSe_2$ and performed sample characterization. All of the authors discussed results, wrote, and commented on the paper.

Notes

The authors declare no competing financial interest.

ACKNOWLEDGMENTS

Y.X.L., C.J.W., S.H.H., V.N.M., and C.L.W. gratefully acknowledge the financial support of this work by the National Science Foundation through Grant no. CMMI-1930881. These authors also acknowledge funding support from Mid-America Transportation Center and Missouri Department of Transportation. D.Z. and B.L. acknowledge the Villanova University startup fund.

REFERENCES

(1) Naguib, M.; Mochalin, V. N.; Barsoum, M. W.; Gogotsi, Y. 25th Anniversary Article: MXenes: A New Family of Two-Dimensional Materials. *Adv. Mater.* **2014**, *26*, 992−1005.

(2) Jiang, X.; Kuklin, A. V.; Baev, A.; Ge, Y.; Ågren, H.; Zhang, H.; Prasad, P. N. Two-dimensional MXenes: From Morphological to Optical, Electric, and Magnetic Properties and Applications. *Phys. Rep.* **2020**, *848*, 1−58.

(3) Naguib, M.; Mashtalir, O.; Carle, J.; Presser, V.; Lu, J.; Hultman, L.; Gogotsi, Y.; Barsoum, M. W. Two-Dimensional Transition Metal Carbides. *ACS Nano* **2012**, *6*, 1322−1331.

(4) Naguib, M.; Kurtoglu, M.; Presser, V.; Lu, J.; Niu, J.; Heon, M.; Hultman, L.; Gogotsi, Y.; Barsoum, M. W. Two-Dimensional Nanocrystals Produced by Exfoliation of Ti_3AlC_2. *Adv. Mater.* **2011**, *23*, 4248−4253.

(5) Zhu, J.; Ha, E.; Zhao, G.; Zhou, Y.; Huang, D.; Yue, G.; Hu, L.; Sun, N.; Wang, Y.; Lee, L. Y.; et al. Recent Advance in MXenes: A Promising 2D Material for Catalysis, Sensor and Chemical Adsorption. *Coord. Chem. Rev.* **2017**, *352*, 306−327.

(6) Maleski, K.; Mochalin, V. N.; Gogotsi, Y. Dispersions of Two-Dimensional Titanium Carbide MXene in Organic Solvents. *Chem. Mater.* **2017**, *29*, 1632−1640.

(7) Ma, R.; Sasaki, T. Two-Dimensional Oxide and Hydroxide Nanosheets: Controllable High-Quality Exfoliation, Molecular Assembly, and Exploration of Functionality. *Acc. Chem. Res.* **2015**, *48*, 136−143.

(8) Wang, Q.; Wang, S.; Guo, X.; Ruan, L.; Wei, N.; Ma, Y.; Li, J.; Wang, M.; Li, W.; Zeng, W. MXene-Reduced Graphene Oxide Aerogel for Aqueous Zinc-Ion Hybrid Supercapacitor with Ultralong Cycle Life. *Adv. Electron. Mater.* **2019**, *5*, No. 1900537.

(9) Deng, W.; Huang, H.; Jin, H.; Li, W.; Chu, X.; Xiong, D.; Yan, W.; Chun, F.; Xie, M.; Luo, C.; et al. All-Sprayed-Processable, Large-Area, and Flexible Perovskite/MXene-Based Photodetector Arrays for Photocommunication. *Adv. Opt. Mater.* **2019**, *7*, No. 1801521.

(10) Guo, Z.; Miao, N.; Zhou, J.; Sa, B.; Sun, Z. Strain-Mediated Type-I/Type-II Transition in MXene/Blue Phosphorene Van Der Waals Heterostructures for Flexible Optical/Electronic Devices. *J. Mater. Chem. C* **2017**, *5*, 978−984.

(11) Hantanasirisakul, K.; Zhao, M. Q.; Urbankowski, P.; Halim, J.; Anasori, B.; Kota, S.; Ren, C. E.; Barsoum, M. W.; Gogotsi, Y. Fabrication of $Ti_3C_2T_x$ MXene Transparent Thin Films with Tunable Optoelectronic Properties. *Adv. Electron. Mater.* **2016**, *2*, No. 1600050.

(12) Mariano, M.; Mashtalir, O.; Antonio, F. Q.; Ryu, W.-H.; Deng, B.; Xia, F.; Gogotsi, Y.; Taylor, A. D. Solution-Processed Titanium Carbide MXene Films Examined as Highly Transparent Conductors. *Nanoscale* **2016**, *8*, 16371−16378.

(13) Salles, P.; Pinto, D.; Hantanasirisakul, K.; Maleski, K.; Shuck, C. E.; Gogotsi, Y. Electrochromic Effect in Titanium Carbide MXene Thin Films Produced by Dip-Coating. *Adv. Funct. Mater.* **2019**, *29*, No. 1809223.

(14) Yang, Q.; Guo, Y.; Yan, B.; Wang, C.; Liu, Z.; Huang, Z.; Wang, Y.; Li, Y.; Li, H.; Song, L.; et al. Hydrogen-Substituted Graphdiyne Ion Tunnels Directing Concentration Redistribution for Commercial-Grade Dendrite-Free Zinc Anodes. *Adv. Mater.* **2020**, *32*, No. 2001755.

(15) Yi, J.; Du, L.; Li, J.; Yang, L.; Hu, L.; Huang, S.; Dong, Y.; Miao, L.; Wen, S.; Mochalin, V. N.; et al. Unleashing the Potential of Ti_2CT_x MXene as A Pulse Modulator for Mid-Infrared Fiber Lasers. *2D Mater.* **2019**, *6*, No. 045038.

(16) Li, G.; Amer, N.; Hafez, H. A.; Huang, S.; Turchinovich, D.; Mochalin, V. N.; Hegmann, F. A.; Titova, L. V. Dynamical Control over Terahertz Electromagnetic Interference Shielding with 2D $Ti_3C_2T_y$ MXene by Ultrafast Optical Pulses. *Nano Lett.* **2020**, *20*, 636−643.

(17) Yi, J.; Li, J.; Huang, S.; Hu, L.; Miao, L.; Zhao, C.; Wen, S.; Mochalin, V. N.; Rao, A. M. Ti_2CT_x MXene-Based All-Optical Modulator. *InfoMat* **2020**, *2*, 601−609.

(18) Yan, J.; Ren, C. E.; Maleski, K.; Hatter, C. B.; Anasori, B.; Urbankowski, P.; Sarycheva, A.; Gogotsi, Y. Flexible MXene/Graphene Films for Ultrafast Supercapacitors with Outstanding Volumetric Capacitance. *Adv. Funct. Mater.* **2017**, *27*, No. 1701264.

(19) Yue, Y.; Liu, N.; Ma, Y.; Wang, S.; Liu, W.; Luo, C.; Zhang, H.; Cheng, F.; Rao, J.; Hu, X.; et al. Highly Self-Healable 3D

Microsupercapacitor with MXene−Graphene Composite Aerogel. *ACS Nano* **2018**, *12*, 4224−4232.
(20) Couly, C.; Alhabeb, M.; Van Aken, K. L.; Kurra, N.; Gomes, L.; Navarro-Suárez, A. M.; Anasori, B.; Alshareef, H. N.; Gogotsi, Y. Asymmetric Flexible MXene-Reduced Graphene Oxide Micro-Supercapacitor. *Adv. Electron. Mater.* **2018**, *4*, No. 1700339.
(21) Zhang, C.; Anasori, B.; Seral-Ascaso, A.; Park, S. H.; McEvoy, N.; Shmeliov, A.; Duesberg, G. S.; Coleman, J. N.; Gogotsi, Y.; Nicolosi, V. Transparent, Flexible, and Conductive 2D Titanium Carbide (MXene) Films with High Volumetric Capacitance. *Adv. Mater.* **2017**, *29*, No. 1702678.
(22) Salles, P.; Quain, E.; Kurra, N.; Sarycheva, A.; Gogotsi, Y. Automated Scalpel Patterning of Solution Processed Thin Films for Fabrication of Transparent MXene Microsupercapacitors. *Small* **2018**, *14*, No. 1802864.
(23) Zhang, C.; Kremer, M. P.; Seral-Ascaso, A.; Park, S. H.; McEvoy, N.; Anasori, B.; Gogotsi, Y.; Nicolosi, V. Stamping of Flexible, Coplanar Micro-Supercapacitors Using MXene Inks. *Adv. Funct. Mater.* **2018**, *28*, No. 1705506.
(24) Zhang, C.; McKeon, L.; Kremer, M. P.; Park, S.-H.; Ronan, O.; Seral-Ascaso, A.; Barwich, S.; Coileáin, C. Ó.; McEvoy, N.; Nerl, H. C.; et al. Additive-Free MXene Inks and Direct Printing of Micro-Supercapacitors. *Nat. Commun.* **2019**, *10*, No. 1795.
(25) Zhang, J.; Seyedin, S.; Gu, Z.; Yang, W.; Wang, X.; Razal, J. M. MXene: A Potential Candidate for Yarn Supercapacitors. *Nanoscale* **2017**, *9*, 18604−18608.
(26) Pang, J.; Mendes, R. G.; Bachmatiuk, A.; Zhao, L.; Ta, H. Q.; Gemming, T.; Liu, H.; Liu, Z.; Rummeli, M. H. Applications of 2D MXenes in Energy Conversion and Storage Systems. *Chem. Soc. Rev.* **2019**, *48*, 72−133.
(27) Li, R.; Zhang, L.; Shi, L.; Wang, P. MXene Ti_3C_2: An Effective 2D Light-to-Heat Conversion Material. *ACS Nano* **2017**, *11*, 3752−3759.
(28) Yu, H.; Wang, Y.; Jing, Y.; Ma, J.; Du, C. F.; Yan, Q. Surface Modified MXene-Based Nanocomposites for Electrochemical Energy Conversion and Storage. *Small* **2019**, *15*, No. 1901503.
(29) Lin, P.; Xie, J.; He, Y.; Lu, X.; Li, W.; Fang, J.; Yan, S.; Zhang, L.; Sheng, X.; Chen, Y. MXene Aerogel-Based Phase Change Materials toward Solar Energy Conversion. *Sol. Energy Mater. Sol. Cells* **2020**, *206*, No. 110229.
(30) Pomerantseva, E.; Gogotsi, Y. Two-Dimensional Heterostructures for Energy Storage. *Nat. Energy* **2017**, *2*, No. 17089.
(31) Fan, Z.; Wang, Y.; Xie, Z.; Wang, D.; Yuan, Y.; Kang, H.; Su, B.; Cheng, Z.; Liu, Y. Modified MXene/Holey Graphene Films for Advanced Supercapacitor Electrodes with Superior Energy Storage. *Adv. Sci.* **2018**, *5*, No. 1800750.
(32) Xu, S.; Wei, G.; Li, J.; Han, W.; Gogotsi, Y. Flexible MXene−Graphene Electrodes with High Volumetric Capacitance for Integrated Co-Cathode Energy Conversion/Storage devices. *J. Mater. Chem. A* **2017**, *5*, 17442−17451.
(33) Anasori, B.; Lukatskaya, M. R.; Gogotsi, Y. 2D Metal Carbides and Nitrides (MXenes) for Energy Storage. *Nat. Rev. Mater.* **2017**, *2*, No. 16098.
(34) Xiong, D.; Li, X.; Bai, Z.; Lu, S. Recent Advances in Layered $Ti_3C_2T_x$ MXene for Electrochemical Energy Storage. *Small* **2018**, *14*, No. 1703419.
(35) Sun, S.; Liao, C.; Hafez, A. M.; Zhu, H.; Wu, S. Two-dimensional MXenes for Energy Storage. *Chem. Eng. J.* **2018**, *338*, 27−45.
(36) Jun, B.-M.; Kim, S.; Heo, J.; Park, C. M.; Her, N.; Jang, M.; Huang, Y.; Han, J.; Yoon, Y. Review of MXenes as New Nanomaterials for Energy Storage/Delivery and Selected Environmental Applications. *Nano Res.* **2019**, *12*, 471−487.
(37) Nan, J.; Guo, X.; Xiao, J.; Li, X.; Chen, W.; Wu, W.; Liu, H.; Wang, Y.; Wu, M.; Wang, G. Nanoengineering of 2D MXene-Based Materials for Energy Storage Applications. *Small* **2019**, No. 1902085.
(38) Li, R.; Sun, W.; Zhan, C.; Kent, P. R.; Jiang, D.-E. Interfacial and Electronic Properties of Heterostructures of MXene and Graphene. *Phys. Rev. B* **2019**, *99*, No. 085429.
(39) Yuan, H.; Li, Z. Interfacial Properties of Black Phosphorus/Transition Metal Carbide Van Der Waals Heterostructures. *Front. Phys.* **2018**, *13*, No. 138103.
(40) Lorencova, L.; Gajdosova, V.; Hroncekova, S.; Bertok, T.; Jerigova, M.; Velic, D.; Sobolciak, P.; Krupa, I.; Kasak, P.; Tkac, J. Electrochemical Investigation of Interfacial Properties of $Ti_3C_2T_x$ MXene modified by aryldiazonium betaine derivatives. *Front. Chem.* **2020**, *8*, 553.
(41) Boddison-Chouinard, J.; Scarfe, S.; Watanabe, K.; Taniguchi, T.; Luican-Mayer, A. Flattening Van Der Waals Heterostructure Interfaces by Local Thermal Treatment. *Appl. Phys. Lett.* **2019**, *115*, No. 231603.
(42) Li, B.; Yin, J.; Liu, X.; Wu, H.; Li, J.; Li, X.; Guo, W. Probing Van Der Waals Interactions at Two-Dimensional Heterointerfaces. *Nat. Nanotechnol.* **2019**, *14*, 567−572.
(43) Rokni, H.; Lu, W. Direct Measurements of Interfacial Adhesion in 2D Materials and Van Der Waals Heterostructures in Ambient Air. *Nat. Commun.* **2020**, *11*, No. 5607.
(44) Wen, Y.; Chen, J.; Guo, Y.; Wu, B.; Yu, G.; Liu, Y. Multilayer Graphene-Coated Atomic Force Microscopy Tips for Molecular Junctions. *Adv. Mater.* **2012**, *24*, 3482−3485.
(45) Lanza, M.; Bayerl, A.; Gao, T.; Porti, M.; Nafria, M.; Jing, G.; Zhang, Y.; Liu, Z.; Duan, H. Graphene-Coated Atomic Force Microscope Tips for Reliable Nanoscale Electrical Characterization. *Adv. Mater.* **2013**, *25*, 1440−1444.
(46) Shim, W.; Brown, K. A.; Zhou, X.; Rasin, B.; Liao, X.; Mirkin, C. A. Multifunctional Cantilever-Free Scanning Probe Arrays Coated with Multilayer Graphene. *Proc. Natl. Acad. Sci. U.S.A.* **2012**, *109*, 18312−18317.
(47) Pacios, M.; Hosseini, P.; Fan, Y.; He, Z.; Krause, O.; Hutchison, J.; Warner, J. H.; Bhaskaran, H. Direct Manufacturing of Ultrathin Graphite on Three-Dimensional Nanoscale Features. *Sci. Rep.* **2016**, *6*, No. 22700.
(48) Hui, F.; Vajha, P.; Shi, Y.; Ji, Y.; Duan, H.; Padovani, A.; Larcher, L.; Li, X. R.; Xu, J. J.; Lanza, M. Moving Graphene Devices from Lab to Market: Advanced Graphene-Coated Nanoprobes. *Nanoscale* **2016**, *8*, 8466−8473.
(49) Dong, Y.; Chertopalov, S.; Maleski, K.; Anasori, B.; Hu, L.; Bhattacharya, S.; Rao, A. M.; Gogotsi, Y.; Mochalin, V. N.; Podila, R. Saturable Absorption in 2D Ti_3C_2 MXene Thin Films for Passive Photonic Diodes. *Adv. Mater.* **2018**, *30*, No. 1705714.
(50) Li, Y.; Huang, S.; Wei, C.; Wu, C.; Mochalin, V. N. Adhesion of Two-Dimensional Titanium Carbides (MXenes) and Graphene to Silicon. *Nat. Commun.* **2019**, *10*, No. 3014.
(51) Jacobs, T. D.; Ryan, K. E.; Keating, P. L.; Grierson, D. S.; Lefever, J. A.; Turner, K. T.; Harrison, J. A.; Carpick, R. W. The Effect of Atomic-Scale Roughness on the Adhesion of Nanoscale Asperities: A Combined Simulation and Experimental Investigation. *Tribol. Lett.* **2013**, *50*, 81−93.
(52) Jiang, T.; Zhu, Y. Measuring Graphene Adhesion Using Atomic Force Microscopy with A Microsphere Tip. *Nanoscale* **2015**, *7*, 10760−10766.
(53) Jung, C.; Kim, S. M.; Moon, H.; Han, G.; Kwon, J.; Hong, Y. K.; Omkaram, I.; Yoon, Y.; Kim, S.; Park, J. Highly Crystalline CVD-Grown Multilayer $MoSe_2$ Thin Film Transistor for Fast Photodetector. *Sci. Rep.* **2015**, *5*, No. 15313.
(54) Rabinovich, Y. I.; Adler, J. J.; Ata, A.; Singh, R. K.; Moudgil, B. M. Adhesion between Nanoscale Rough Surfaces: I. Role of Asperity Geometry. *J. Colloid Interface Sci.* **2000**, *232*, 10−16.
(55) Gong, P.; Li, Q.; Liu, X.-Z.; Carpick, R. W.; Egberts, P. Adhesion Mechanics between Nanoscale Silicon Oxide Tips and Few-Layer Graphene. *Tribol. Lett.* **2017**, *65*, No. 61.
(56) Hart, J. L.; Hantanasirisakul, K.; Lang, A. C.; Anasori, B.; Pinto, D.; Pivak, Y.; van Omme, J. T.; May, S. J.; Gogotsi, Y.; Taheri, M. L. Control of MXenes' Electronic Properties Through Termination and Intercalation. *Nat. Commun.* **2019**, *10*, No. 522.
(57) Persson, I.; Halim, J.; Hansen, T. W.; Wagner, J. B.; Darakchieva, V.; Palisaitis, J.; Rosen, J.; Persson, P. O. How much

https://dx.doi.org/10.1021/acsami.0c18624
ACS Appl. Mater. Interfaces 2021, 13, 4682−4691

Oxygen Can A MXene Surface Take before It Breaks? *Adv. Funct. Mater.* **2020**, *30*, No. 1909005.
(58) Huang, S.; Mochalin, V. N. Hydrolysis of 2D Transition-Metal Carbides (MXenes) in Colloidal Solutions. *Inorg. Chem.* **2019**, *58*, 1958−1966.
(59) Zhou, D.; Lang, J.; Yoo, N.; Unocic, R. R.; Wu, Q.; Li, B. Fluid Guided CVD Growth for Large-Scale Monolayer Two-Dimensional Materials. *ACS Appl. Mater. Interfaces* **2020**, *12*, 26342−26349.
(60) Malard, L.; Pimenta, M. A.; Dresselhaus, G.; Dresselhaus, M. Raman Spectroscopy in Graphene. *Phys. Rep.* **2009**, *473*, 51−87.
(61) Tongay, S.; Zhou, J.; Ataca, C.; Lo, K.; Matthews, T. S.; Li, J.; Grossman, J. C.; Wu, J. Thermally Driven Crossover from Indirect toward Direct Bandgap in 2D Semiconductors: $MoSe_2$ versus MoS_2. *Nano Lett.* **2012**, *12*, 5576−5580.
(62) Utama, M. I. B.; Lu, X.; Zhan, D.; Ha, S. T.; Yuan, Y.; Shen, Z.; Xiong, Q. Etching-Free Patterning Method for Electrical Characterization of Atomically Thin $MoSe_2$ Films Grown by Chemical Vapor Deposition. *Nanoscale* **2014**, *6*, 12376−12382.
(63) Lee, L. T. L.; He, J.; Wang, B.; Ma, Y.; Wong, K. Y.; Li, Q.; Xiao, X.; Chen, T. Few-Layer $MoSe_2$ Possessing High Catalytic Activity towards Iodide/Tri-Iodide Redox Shuttles. *Sci. Rep.* **2014**, *4*, No. 4063.
(64) Li, P.; You, Z.; Cui, T. Adhesion Energy of Few Layer Graphene Characterized by Atomic Force Microscope. *Sens. Actuators, A* **2014**, *217*, 56−61.
(65) Suk, J. W.; Na, S. R.; Stromberg, R. J.; Stauffer, D.; Lee, J.; Ruoff, R. S.; Liechti, K. M. Probing the Adhesion Interactions of Graphene on Silicon Oxide by Nanoindentation. *Carbon* **2016**, *103*, 63−72.

https://dx.doi.org/10.1021/acsami.0c18624
ACS Appl. Mater. Interfaces 2021, 13, 4682−4691